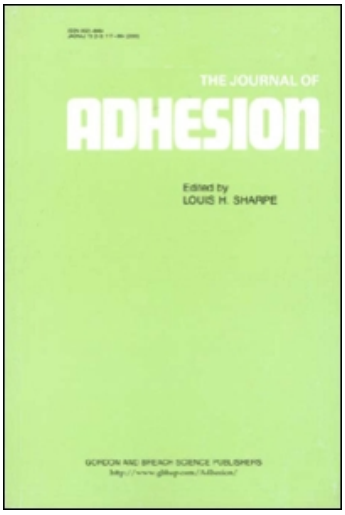

The Journal of Adhesion
Publication details, including instructions for authors and subscription information:
http://www.informaworld.com/smpp/title~content=t713453635

Molecular structure of interfaces formed with plasma-polymerized silica-like primer films: Part II. Characterization of the primer/metal interface using x-ray photoelectron spectroscopy in SITU

R. H. Turner[a]; F. J. Boerio[a]
[a] Department of Materials Science and Engineering, University of Cincinnati, Cincinnati, OH, USA

Online publication date: 08 September 2010

To cite this Article Turner, R. H. and Boerio, F. J.(2002) 'Molecular structure of interfaces formed with plasma-polymerized silica-like primer films: Part II. Characterization of the primer/metal interface using x-ray photoelectron spectroscopy in SITU', The Journal of Adhesion, 78: 6, 465 — 493
To link to this Article: DOI: 10.1080/00218460213730
URL: http://dx.doi.org/10.1080/00218460213730

The Journal of Adhesion, 78: 465–493, 2002

0021-8464/02 $12.00 +.00
DOI: 10.1080/00218460290010377

MOLECULAR STRUCTURE OF INTERFACES FORMED WITH PLASMA-POLYMERIZED SILICA-LIKE PRIMER FILMS: PART II. CHARACTERIZATION OF THE PRIMER/METAL INTERFACE USING X-RAY PHOTOELECTRON SPECTROSCOPY IN SITU

R. H. Turner
F. J. Boerio
Department of Materials Science and Engineering,
University of Cincinnati, Cincinnati, OH, USA

X-ray photoelectron spectroscopy (XPS) was performed in situ on plasma-polymerized silica-like films that were deposited onto metal substrates. Relatively thick films (~8.0 nm) had spectra that were typical of bulk amorphous silicon dioxide (a-SiO_2). When thinner films were analyzed (~2.4 nm), a Si(2p) peak emerged that was due to the formation of silicon suboxide at the interface. Changes in the metal and metal oxide peaks showed that oxidation of the substrates during plasma etching and deposition occurred. It was determined that during the initial stages of plasma deposition, metal atoms from the substrate migrated to the metal-oxide surface. This resulted in preferential oxidation of metal atoms with the formation of silicon suboxide at the film/metal interface. In addition, interfacial suboxide formation was shown to have a dependence upon the diffusivity of the metal substrate atoms through the surface oxide of the metal. As a result, more interfacial suboxide was observed to form for depositions on titanium substrates in comparison with depositions on aluminum substrates. A detailed analysis of the atomic species detected with in situ XPS enabled us to develop a model of the molecular structure at the a-SiO_2/metal interface for plasma depositions on aluminum and titanium substrates. When the possible chemical reaction routes for film deposition were considered, the formation of primary Al-O-Si and Ti-O-Si bonds at the interface was proposed.

Keywords: Plasma-polymerized films; Interfacial analysis; Suboxide; a-SiO_2 defects; In situ X-ray photoelectron spectroscopy; Aluminum; Titanium

Received 17 August 2001; in final form 28 February 2002.

This work was funded in part by the National Science Foundation.

Present address of Robert H. Turner is The Proctor and Gamble Co., S-225 BRTC-NPT, 8611 Beckett Road, West Chester, OH 45069, USA.

Address correspondence to F. James Boerio, Department of Materials Science and Engineering, University of Cincinnati, Cincinnati, OH 45221-0012, USA. E-mail: fboerio@uceng.uc.edu

INTRODUCTION

The molecular structures of the interfaces formed between plasma-polymerized amorphous silica-like (a-SiO_2) films and metal substrates are of significant importance when using these films as primers for promoting strong and durable adhesive bonds. The goal of this research was to determine the molecular structure of the a-SiO_2/metal interface for a-SiO_2 films deposited onto aluminum and titanium substrates. In Part I of this work, the a-SiO_2/metal interface was investigated using in situ reflection-absorption infrared spectroscopy (RAIR). Thin films of a-SiO_2 were deposited and analyzed with in situ RAIR in order to eliminate the effects of atmospheric contamination and hydration. It was found that during the initial stages of plasma deposition, a suboxide species of silicon was formed at the a-SiO_2/metal interface. It was also shown that the suboxide was formed due to plasma-assisted reactions between the metal substrate and the depositing film. In this paper, the molecular structure at the a-SiO_2/metal interface was further analyzed in situ using X-ray photo electron spectroscopy (XPS). By using in situ XPS, which complimented in situ RAIR, a more detailed analysis of the molecular structure at the a-SiO_2/metal interface was developed. In Part III, the mechanical strength and durability of the a-SiO_2/metal substrate interface was investigated and correlated with the findings in Parts I and II.

XPS can be used to investigate buried interfaces as long as the overlayer does not prevent photoelectrons from escaping the interfacial region. The Si(2p) photoelectrons that are generated by Mg Kα X-rays have a kinetic energy of approximately 1150 eV and an inelastic mean free path of 2.1–2.5 nm in a-SiO_2 [1]. Although the true kinetic energy of photoelectrons emitted by an unknown interfacial species may be more or less than this, the maximum film thickness necessary for interfacial analysis can still be estimated. At a low kinetic energy of 100 eV photoelectrons will escape from a-SiO_2 at a 75° take-off angle at depths no more than 2.5 nm (the take-off angle is defined here as the angle formed between the sample surface and the optical axis of the electron analyzer). Certainly, less overlayer will be beneficial since similar to the infrared spectra that were obtained in Part I of this work, a reduction in film thickness will decrease the intensity of features due to the bulk overlayer and at the same time increase the intensity of the features due to the interface. In addition, the features in the spectra due to the interface will intensify relative to the spectral features of the bulk overlayer with increasing take-off angles.

Since the film thickness necessary to study the a-SiO_2 interface must be less than 2.5 nm, these films must be protected from atmospheric contaminants and hydration. One way to overcome atmospheric contamination is to analyze the deposited film in situ. This was achieved by interfacing a specially built plasma reactor to the XPS that enabled the user to transport a film and substrate under vacuum to the ultra-high vacuum (UHV) analysis chamber of the XPS, immediately after deposition.

EXPERIMENTAL

Since the plasma polymerization processes were carried out at $\sim 10^{-1}$ Torr, and the XPS analysis chamber maintains a base pressure of $\sim 10^{-10}$ Torr, it was necessary to have a connecting vacuum chamber that could achieve intermediate vacuum levels. This allowed a sample to be transferred from the plasma reactor to the XPS analysis chamber and vice versa without degrading the base pressure of the XPS analysis chamber. The samples that were used consisted of a substrate mounted on a standard 25 mm diameter XPS sample holder, which could be manipulated within the vacuum system using transfer rods.

Plasma etching and plasma polymerization of a-SiO_2 films was carried out using a specially built plasma reactor that was interfaced to the main analysis chamber of the XPS. Figure 1 shows a side view diagram of the plasma reactor attached to the XPS system. The plasma reactor was constructed with a stainless steel vacuum chamber that had several ports, which were used for a sample holder, sample transfer, pressure measurement, vacuum, monomer inlet, and the plasma applicator. The top of the reactor had an O-ring sealed flange with the plasma applicator mounted onto it. The top-flange with the attached plasma applicator could be easily removed for access to the interior of the reactor for repairs, modifications, or for treating substrates with dimensions slightly larger than those of the XPS sample holder. Argon and oxygen carrier gasses were introduced through a port in the top of the plasma applicator. Monomer was introduced through a separate inlet, located between the plasma applicator and sample substrate, downstream of the active glow discharge. The plasma applicator was constructed by wrapping a copper induction coil around the exterior of a glass envelope and, in order to prevent stray RF radiation, both the induction coil and glass envelope were contained inside an aluminum cylinder. The RF power generator output was connected to the copper induction coil using an automatic matching network designed for inductively coupled loads.

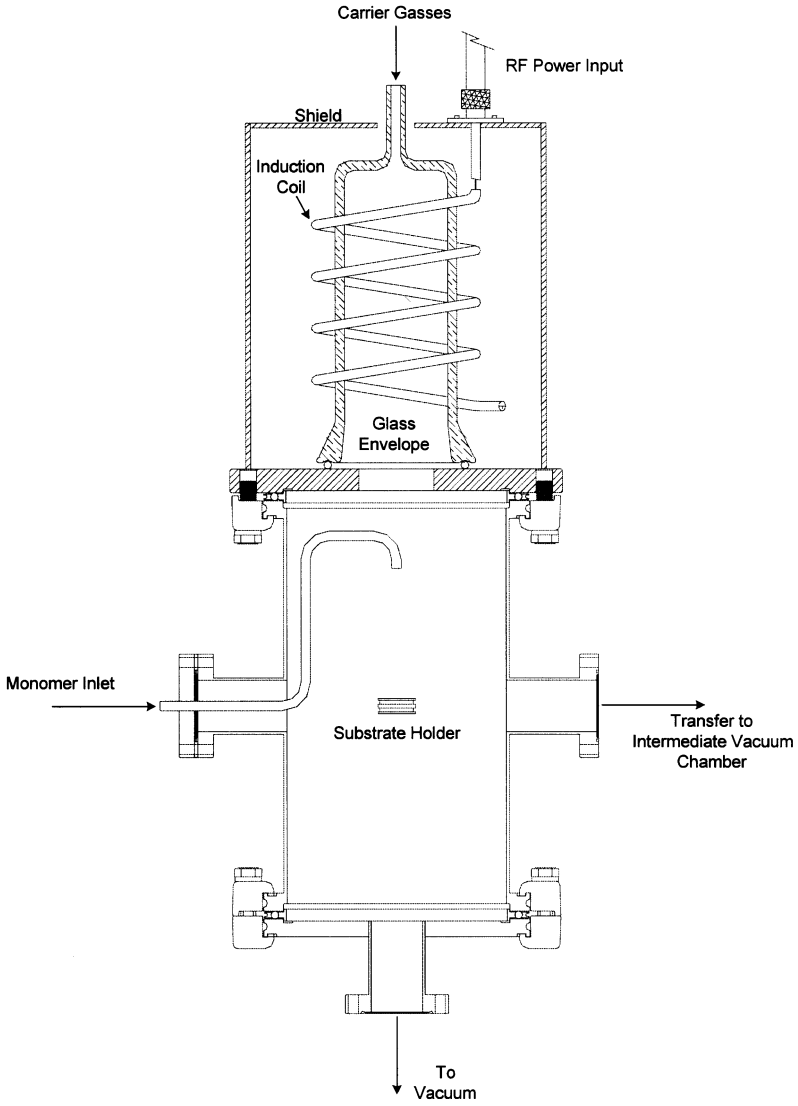

FIGURE 1 Diagram of the in situ plasma reactor interfaced with the XPS system.

A turbo-molecular pump was used to reduce the pressure of the plasma chamber in order to transfer the sample to the intermediate vacuum chamber, which was separated from the plasma chamber by a gate valve. The intermediate vacuum chamber was used to transfer

samples from the relatively high-pressure plasma reactor to the relatively low-pressure XPS chamber, also separated by a gate valve. The intermediate chamber had several ports which were connected to an ion gauge for low-pressure measurement, the turbo-molecular pump, the mechanical pump, and two magnetically coupled linear manipulators with sample holders on their ends for transferring samples. The intermediate chamber was also continuously pumped with an ion pump, so that a base pressure between 10^{-8} and 10^{-9} Torr was maintained.

Aluminum and titanium substrates (14 mm $\times$ 14 mm) were cut from 2024-T3 and Ti-6Al-4V sheet (ca. 2 mm thick), respectively. Samples were rough polished with 600-grit silicon carbide polishing paper and water. The rough polished samples were then polished to a mirror finish by using 6 μm and then 1 μm diamond polishing compounds. After diamond polishing, the samples were rinsed in reagent-grade toluene several times and then blown dry with a stream of nitrogen gas.

A sample substrate was mounted onto the stainless steel XPS sample holder and introduced into the XPS analysis chamber for analysis. After analysis the sample was transferred to the plasma reactor for plasma etching. Plasma etching was carried out for 10 min using 40 standard cm^3 per minute (SCCM) of argon and 10 SCCM of oxygen at 100 Watts RF power while maintaining a pressure of 500 mTorr. After plasma etching, the sample was transferred to the intermediate chamber and then to the UHV analysis chamber of the XPS for analysis.

After analyzing the plasma-etched substrate, the sample was transferred back to the plasma reactor for plasma deposition and then reanalyzed. Plasma polymerization of a-SiO_2 films was carried out for 10 min, 3 min, and 1 min using 100 Watts RF power, 40 SCCM of argon, 10 SCCM of oxygen, and 0.5 SCCM hexamethyldisiloxane (HMDSO), at 500 mTorr pressure. After deposition, the sample was transferred back to the XPS chamber for analysis.

X-ray photoelectron spectra were obtained using a Physical Electronics model 5300 XPS. Spectra were acquired using magnesium K_α radiation, usually at 300 Watts; however, some spectra were acquired using 400 Watts to help resolve weak signals when necessary. Survey and high-resolution spectra were acquired using 89.45 eV and 17.90 eV pass energies, respectively. High-resolution spectra were acquired at 15°, 45°, and 75° take-off angles, where the take-off angle was the angle formed between the optical axis of the electron analyzer and the surface of the sample. The effect of sample charging was eliminated by correcting the observed spectra to yield a C(1s) binding

energy for saturated hydrocarbons equal to 284.6 eV. For most in situ plasma-treated substrates no carbon signal was observed, and charging was corrected by adjusting the position of the metal peak of the substrate to its known literature value. In addition, some samples were transferred to the atmosphere after analysis for a brief contamination period (ca. 20 s) and then reanalyzed. The charging on the adsorbed carbon contaminants was determined and used as a check for the charge correction of the previous analysis.

Optical properties of the substrates and films were determined ex situ after XPS analysis was performed. The films were analyzed using a variable angle spectroscopic ellipsometer (VASE^{TM}) from J. A. Woollam Co. Δ and Ψ values were typically collected at 10 nm intervals in the spectral range 300−1200 nm and from 65° to 80° angle of incidence at 5° intervals. A computer program, WVASE^{TM}, was used to calculate the thickness of the films by performing a least squares fitting of the measured Δ and Ψ values of a model that used optical constants for SiO_2 [2].

RESULTS AND DISCUSSION

Using ellipsometry, the films deposited for 10, 3 and 1 min on aluminum and titanium substrates were determined to be 8.0, 2.4, and 0.8 nm thick, respectively. This corresponded to a deposition rate of about ca. 0.8 nm/min. This deposition rate was comparable with that for the in situ RAIR system, as discussed in Part I of this work.

Figures 2 and 3 show the survey spectra of the as-polished aluminum and titanium substrates, obtained at a 45° take-off angle. Peaks due to oxygen, carbon, and the metal substrate were detected. A significant amount of hydrocarbon contamination was present on the surface of the as-polished metal substrates. Figures 2 and 3 also show the survey spectra of the aluminum and titanium substrates after plasma etching for 10 min, respectively. The carbon C(1s) signals have nearly disappeared due to plasma etching. The additional peaks near 689 eV were due to a slight fluorine contamination of the aluminum and titanium. This contamination occurred due to sputtering of an unknown fluorine source within the plasma reactor during plasma etching, possibly an elusive fluorinated O-ring or residual fluorinated pump oil. The highly reactive fluorine reacted with the metal surface to form inorganic fluorides, a highly stable material. Fluorine contamination has been a tenacious phenomenon for plasma etching of reactive metal substrates, especially for aluminum since the free-energy of formation for aluminum fluoride is high [3].

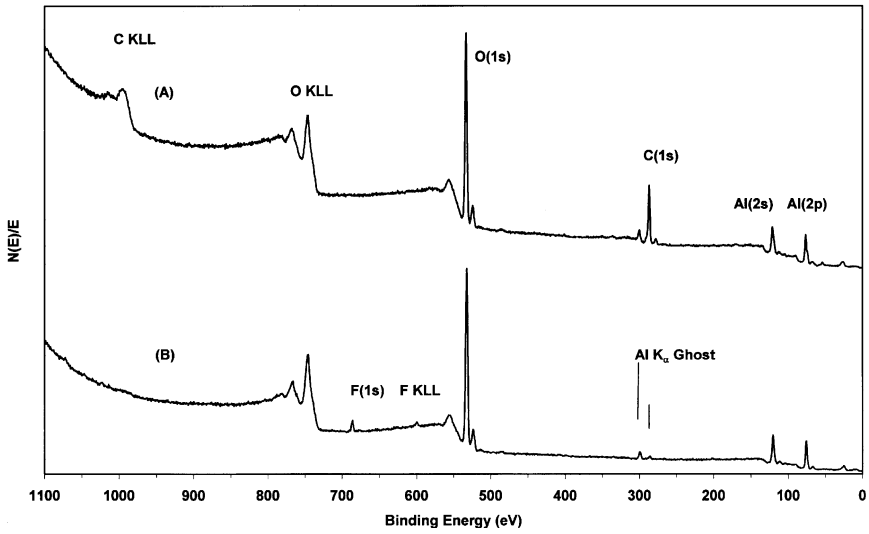

FIGURE 2 In situ XPS survey spectra obtained at a take-off angle of 45° for aluminum substrate (A) as-polished and (B) after plasma etching.

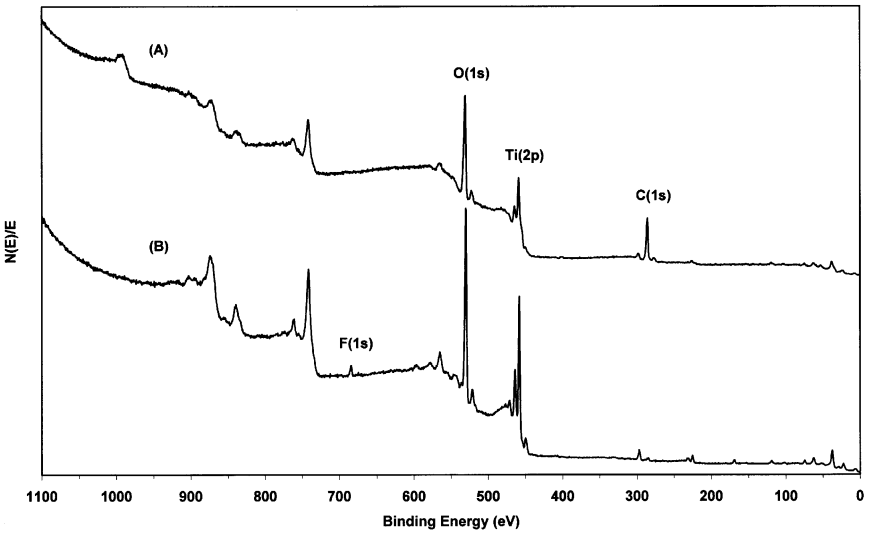

FIGURE 3 In situ XPS survey spectra obtained at a take-off angle of 45° for a titanium substrate (A) as-polished and (B) after plasma etching.

Table 1 shows the atomic concentrations for the elements observed on the metal substrates as-polished and after plasma etching for a take-off angle of 45°. Typically, after plasma etching, only a few atomic percent carbon could be detected on the metal substrates. This indicated that the plasma etching process was very aggressive towards removing virtually all the adsorbed surface contaminants.

The high-resolution Al(2p) and Ti(2p) spectra acquired at a 75° take-off angle for the aluminum and titanium substrates before and after plasma etching are shown in Figures 4 and 5. For the aluminum substrates, two components were used for curve-fitting the spectra, one near 76 eV, and the other near 73 eV. The peak near 76 eV was due to aluminum atoms that had three coordinating oxygen atoms (Al^{+3}) in the oxide and the peak near 73 eV was due to the metallic (Al^0) aluminum atoms [4]. The increase in the peak height ratio, Al^{+3} to Al^0, after plasma etching, was due to plasma-induced oxide formation.

For the Ti(2p) spectra in Figure 5, the strong peak near 458.0 eV was due to the Ti($2p_{3/2}$) of the oxide, Ti^{+4}, and a small peak near 452.6 eV was due to the unoxidized metal, Ti^0. Peaks near 453.6 eV, 455.0 eV, and 456.2 eV represented the intermediate oxidation states of titanium, Ti^{+1}, Ti^{+2}, and Ti^{+3}, respectively [4]. The peak near 463.5 eV was due to Ti($2p_{1/2}$) photoelectrons. Plasma etching significantly reduced the intensities of the metallic peak and those for intermediate oxidation states.

For a given take-off angle, the oxide thickness, d (in nm), can be determined from the relative intensities of the oxide and metallic photoelectron peaks, I_{ox} and I_m, using the relationship shown below [5, 6]:

$$d = \lambda_{ox} \sin(\theta) \ln\left(\frac{N_m \lambda_m}{N_{ox} \lambda_{ox}} \left(\frac{I_{ox}}{I_m}\right) + 1\right). \quad (1)$$

TABLE 1 XPS Atomic Concentrations of Elements Detected as a Function of Take-off Angle for Aluminum Substrates As-polished and After Plasma Etching

Sample	Take-off angle	Atomic concentration (%)			
		C	O	Al	F
As-polished 2024 aluminum	15°	37.6	45.7	16.7	—
	45°	23.8	53.0	23.2	—
	75°	18.9	54.4	26.5	0.2
After plasma etching	15°	2.6	66.3	26.3	4.9
	45°	1.6	65.7	29.2	3.5
	75°	2.0	64.9	30.0	2.9

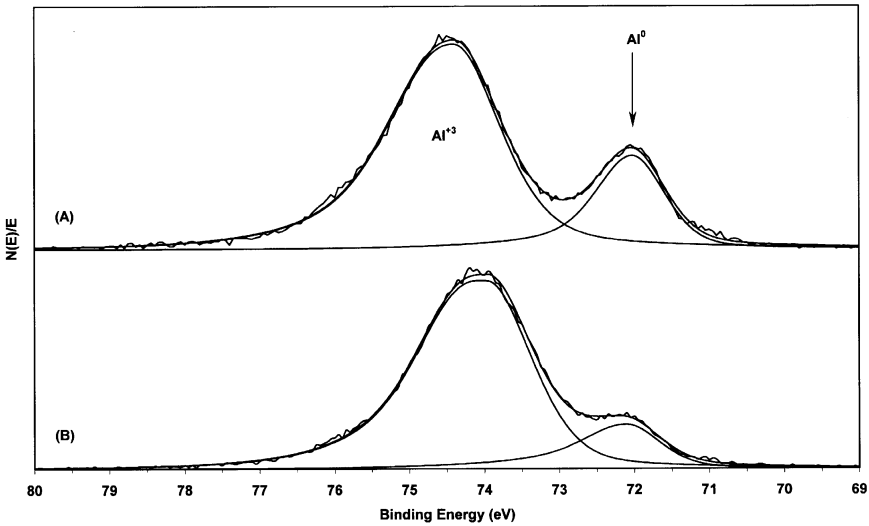

FIGURE 4 High resolution Al(2p) spectra obtained at a 75° take-off angle of an aluminum substrate (A) as-polished and (B) after plasma etching.

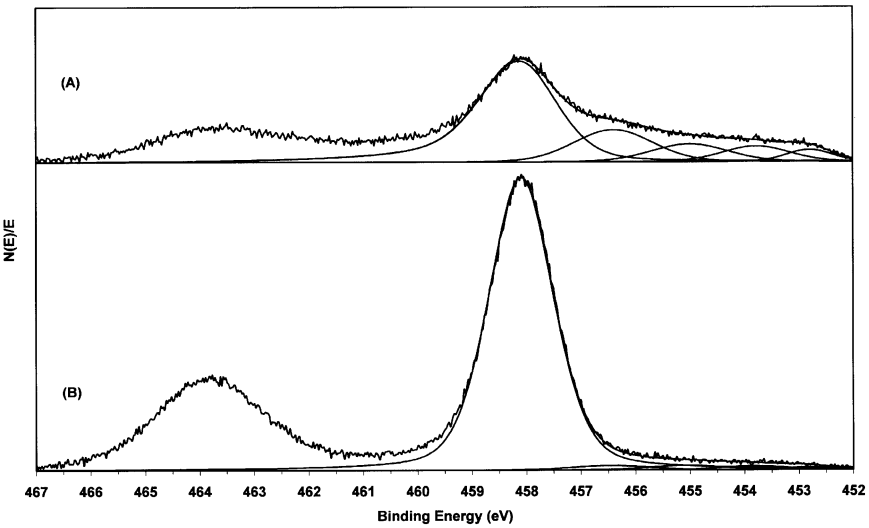

FIGURE 5 High resolution Ti(2p) spectra obtained at a 75° take-off angle for a titanium substrate (A) as-polished and (B) after plasma etching.

N_m and N_{ox} represent the atomic density of atoms in the metal and oxide, respectively, θ is the photoelectron take-off angle between the sample surface and the optical axis of the analyzer, and λ_m and λ_{ox} are the inelastic mean free path (IMFP) values (in nm) of the corresponding photoelectrons in the metal and oxide, respectively. Using Mg K_α X-rays, the IMFP values for the oxide and metal have been determined to be approximately 2.37 nm and 1.82 nm for aluminum, respectively, and 2.07 nm and 1.54 nm for titanium, respectively [7, 8]. The volume density ratio, N_m/N_o, was determined to be approximately 1.31 for aluminum and 1.76 for titanium [9]. Using these material constants, Equation (1) indicated that the oxide thickness on the aluminum substrates was 2.0 nm for the as-polished substrate and 3.0 nm after plasma etching. For the as-polished titanium substrate, the ambient-formed oxide was calculated to be 2.9 nm thick, which was in good agreement with the values found in the literature [8]. After plasma etching, the titanium oxide was found to be 7.9 nm thick; this indicated that significant oxide growth on the titanium substrate occurred during plasma treatment.

Figure 6 shows the survey spectra obtained at a 45° take-off angle for 10-min depositions on plasma-etched aluminum and titanium

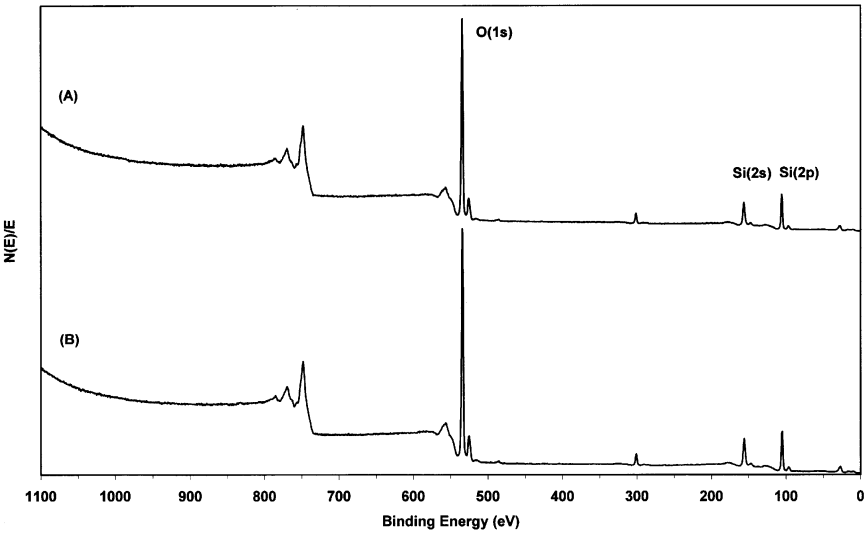

FIGURE 6 XPS survey spectra obtained at a 45° take-off angle for plasma-polymerized a-SiO_2 primer films deposited onto (A) aluminum and (B) titanium substrate.

substrates. Only oxygen and silicon were detected, and since these films had a measured thickness of 8.0 nm, signals due to the substrate were difficult to detect. The films had concentrations of carbon that were less than 1 atomic percent and indicated that the conditions used for plasma polymerization produced highly inorganic a-SiO_2 films. The oxygen-to-silicon ratio for these films was ca. 2.3:1 and indicated that excess oxygen was present due to nonbridging species, such as SiOH.

Figures 7 and 8 show the curve-fit high-resolution Si(2p) spectra obtained at a 45° take-off angle for a-SiO_2 films that were deposited onto aluminum and titanium substrates for different deposition times, respectively. For the 8.0 nm depositions a single peak, located at approximately 103.7 eV, was curve-fit to the spectrum. This single peak was characteristic of silicon in the fully-oxidized state (Si^{+4}) [4, 8]. At this binding energy, each silicon atom had 4 coordinating oxygen atoms, as in crystalline quartz or a-SiO_2. Little variation between Si(2p) collected at different take-off angles was observed for the 8.0 nm depositions. This observation indicated that the chemical structure of the film was fairly consistent within the sampling depth. Figures 7 and 8 clearly show that more than one oxidation state of silicon was detected for films thinner than 8.0 nm. In addition to the Si^{+4} peak at 103.7 eV, a lower binding energy peak near 102.5 eV was

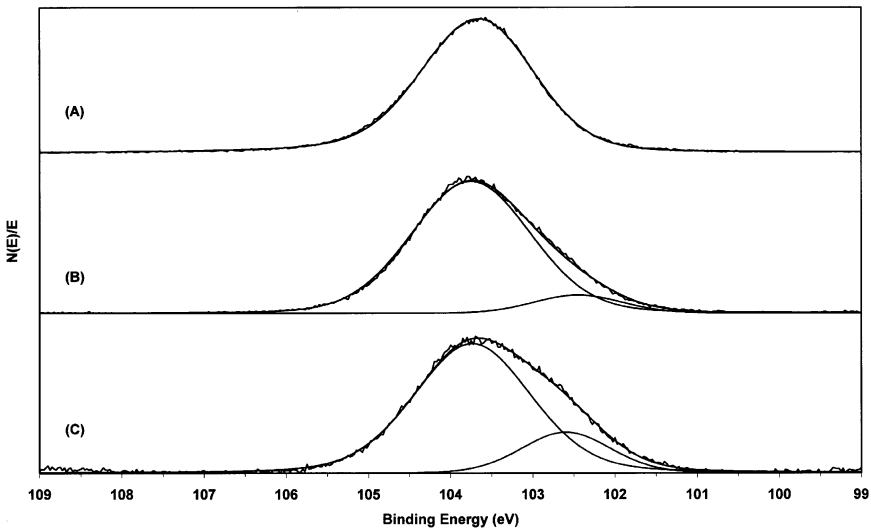

FIGURE 7 High resolution Si(2p) spectra obtained at a 45° take-off angle for (A) 8.0 nm, (B) 2.4 nm, and (C) 0.8 nm a-SiO_2 films deposited onto aluminum substrates.

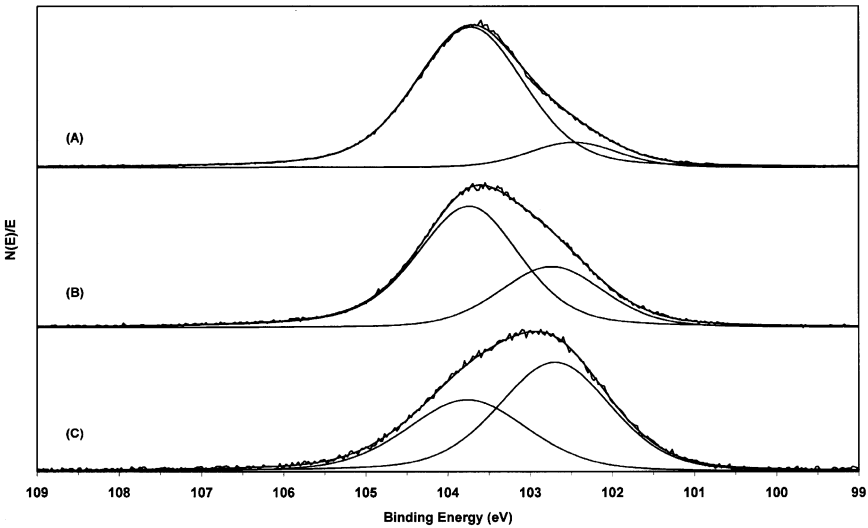

FIGURE 8 High resolution Si(2p) spectra obtained at a 45° take-off angle for (A) 8.0 nm, (B) 2.4 nm, and (C) 0.8 nm a-SiO_2 films deposited onto titanium substrates.

curve-fit to the spectra. This peak was due to silicon atoms with a Si^{+3} oxidation state, a suboxide of silicon, which had three coordinating oxygen atoms. The intensification of the band at 102.5 eV with decreasing film thickness indicated that it was buried beneath an a-SiO_2 overlayer of silicon with Si^{+4} oxidation state. The corresponding C(1s) spectra for all of these depositions showed virtually no signal due to carbon. It was unlikely that the two Si(2p) peaks were due to a differential charging artifact since the separation between them remained independent of film thickness. In addition, the Si-KLL peak (not shown), which was generated with the Bremstralung radiation from the X-ray source, appeared to have only one component, unlike that for a situation involving differential charging.

The peak intensities of the suboxide species in Figures 7 and 8 also show that more suboxide was present for depositions on titanium substrates when compared with depositions on aluminum substrates. This same effect was previously observed by the in situ RAIR analysis of the a-SiO_2/aluminum and titanium interfaces in Part I of this work.

Figures 9 and 10 show the high-resolution curve-fit O(1s) spectra that were obtained at a 45° take-off angle for depositions on aluminum and titanium substrates. For the relatively thick films deposited for

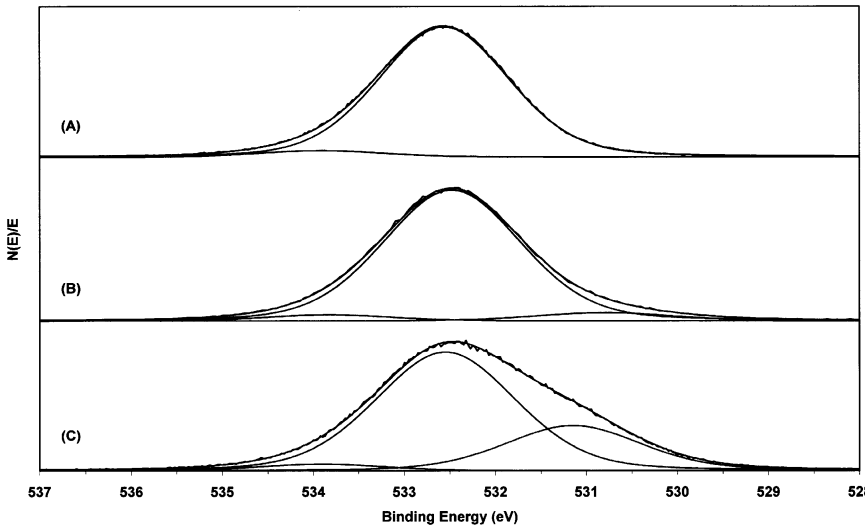

FIGURE 9 High resolution O(1s) spectra obtained at a 45° take-off angle for (A) 8.0 nm, (B) 2.4 nm, and (C) 0.8 nm a-SiO_2 films deposited onto aluminum substrates.

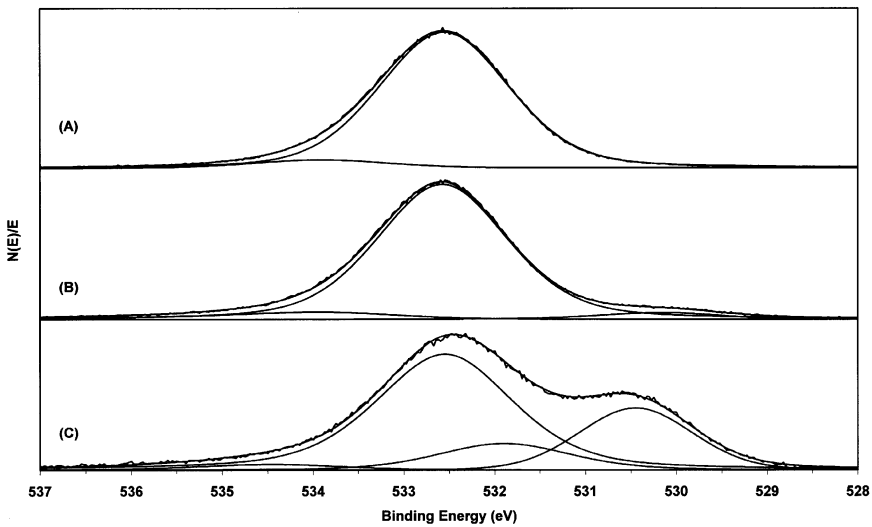

FIGURE 10 High resolution O(1s) spectra obtained at a 45° take-off angle for (A) 8.0 nm, (B) 2.4 nm, and (C) 0.8 nm a-SiO_2 films deposited onto titanium substrates.

10 min, the main peak at 532.5 eV was due to the oxygen atoms (O^{2-}) in the a-SiO_2 film that were coordinated with two silicon atoms, i.e., bridging oxygen atoms [4, 8]. The smaller peak at 534.7 eV was due to hydroxyl groups (OH). No significant variation in the curve-fit intensities were observed for different take-off angles, and this indicated that the chemical structure of the film was consistent within the sampling depth. As thinner a-SiO_2 films were analyzed, signals due to the underlying metal oxide were observed.

The XPS results confirmed that the previously assigned IR peak at 1090 cm^{-1} was due to suboxide and not strained Si-O-Si bonds. It has been shown that the geometrical aspects of Si-O-Si bonds have little effect on XPS spectra. Variations in the Si-O-Si bond angle, and to a lesser extent the Si-O bond length, will only result in slight (ca. 0.5 eV) variations in the FWHM values of the Si(2p) peak components [10].

The in situ XPS results also supported the in situ infrared results in that the oxidation of the aluminum and titanium substrates occurred at the expense of reducing the a-SiO_2 at the interface, or at least by inhibiting full oxidation of the initially adsorbed monomer species. However, unlike the infrared results, the XPS results showed that very little carbon resided at the a-SiO_2/aluminum interface. Although the infrared results supported the formation of suboxides that were due to silicon-carbon bonds, Si-Si bonds, or oxygen vacancy defects ($O_3{\equiv}Si^{\cdot+}Si{\equiv}O_3$), the XPS results only supported suboxide formation due to Si-Si bonds or oxygen vacancies.

Until this point, the suboxide layer at the a-SiO_2/metal interface has not been dimensionally characterized beyond the fact that the results from Part I indicated that it had approximately half as much suboxide at the a-SiO_2/aluminum interface than at the a-SiO_2/titanium interface. Angle-resolved XPS data can be manipulated to give a rough indication of the depth and concentration of an atomic species within a sample by using a fixed value for the IMFP. XPS investigations of compound layer structures with layers of finite thickness and depth have been simulated with varying degrees of success [11–13]. These simulations used mathematical models that were based on the Beer-Lambert law. However, because of certain assumptions, signal attenuation, and diffuse boundaries of layers, XPS layer models have only been able provide a rather qualitative representation of a real sample, and the depths of atomic species can only be relatively considered [13]. For the simple situation of a substrate with one buried layer, the X-ray photoelectron intensities of atoms in the buried layer, collected at different take-off angles, must obey the following relationship [11]:

$$F_i(\theta, d, t, \lambda) = e^{\frac{-d}{\lambda \sin(\theta)}}\left(1 - e^{\frac{-t}{\lambda \sin(\theta)}}\right), \quad (2)$$

where F_i is the atomic concentration (percent) of an atomic species having a chemical state i, is assumed to be fully concentrated within the layer buried at depth, d has a thickness of t, and λ is the IMFP of photoelectrons from the atomic species, i, within the buried layer and has been assumed to be similar to its IMFP within the overlayer. The atomic concentration of a species, F_i, can be obtained as a function of spectrometer take-off angle, θ. For this study, the total thickness of the a-SiO_2 film was known and assumed to be the sum of the suboxide layer thickness, t, and depth, d. Equation (2) was solved for layer depth and thickness using the measured fractions of the suboxide peak in the Si(2p) spectra obtained at various take-off angles. Figure 11 shows a graphical representation of the solutions for Equation (1) using the data points obtained for the 2.4 nm depositions on aluminum and titanium substrates. The results indicated that a buried layer of Si^{+3} suboxide was formed at the a-SiO_2/metal substrate interface that was 1.0 nm below the surface of the a-SiO_2 film for depositions on titanium substrate and 1.4 nm below the surface for depositions on aluminum substrates. These layers had thickness values of 1.0 nm (i.e., 3 layers of a-SiO_2) for the deposition on

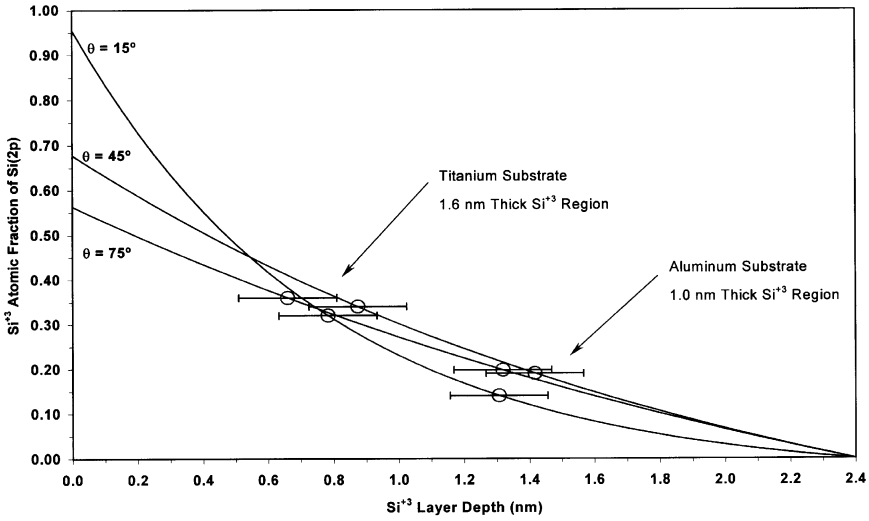

FIGURE 11 Atomic fractions, F, for the Si^{+3} species detected at 15°, 45°, and 75° take-off angles, plotted against layer depth, d, for a 2.4-nm thick a-SiO_2 film deposited onto aluminum and titanium substrates.

aluminum and 1.6 nm (i.e., 5 layers of a-SiO_2) for the deposition on titanium. A standard error of ± 0.15 nm was applied to each data point, which corresponded to one-half the thickness of a monolayer of a-SiO_2 [1]. The data points for each take-off angle agreed to within one monolayer of a-SiO_2. In addition, the thickness values of the suboxide regions agreed with the infrared results, which showed that nearly twice as much suboxide was formed for depositions on titanium substrates as compared with depositions on aluminum substrates.

When the XPS data collected for the 0.8-nm thick a-SiO_2 films was applied to Equation (2), the average depth value obtained for depositions on titanium was negative, and it was zero for depositions on aluminum. These nonphysical results were consistent with the results obtained for the 2.4 nm depositions, since a buried layer was not produced for a 0.8-nm thick film.

Since the suboxide region at the a-SiO_2/metal interface was at least 1.0 nm thick, the 0.8 nm depositions had a molecular structure similar to the suboxide layer. Both Si^{+3} and Si^{+4} species were detected for the 0.8 nm depositions, indicating that the suboxide regions were a dispersion of both silicon species. The 0.8 nm layer of Si^{+3} and Si^{+4} species had a chemistry that was proportional to their Si(2p) band components. As a result, the overall chemistry of the buried suboxide layers can be estimated from the XPS data collected for the 0.8 nm depositions on aluminum and titanium.

In order to determine the molecular structure formed between the metal substrate and the a-SiO_2 film, the chemistry of the metal substrate and the bulk a-SiO_2 film must be determined. The intensities of the curve-fit components at high take-off angles for the oxygen peaks O(1s) and metal peaks Si(2p), Al(2p), and Ti(2p) were used to determine the atomic concentrations of the bulk a-SiO_2 film and the plasma-etched metal oxides of the aluminum and titanium substrates, respectively. Table 2 lists the atomic percentages obtained by XPS for plasma-etched titanium and aluminum substrates along with those for bulklike a-SiO_2 films (8.0 nm) deposited on aluminum and titanium substrates. In addition, XPS data collected for a pure a-SiO_2 (quartz) sample is included for reference. A 5% error, inherent in XPS composition calculations [14], is also listed for each species.

From the atomic compositions listed in Table 2, the chemical formulae for the plasma-etched aluminum and titanium substrates, the 8.0 nm bulklike a-SiO_2 films, and that for a pure a-SiO_2 sample (quartz) were determined, and they are listed in Table 3. The chemical formulae were obtained by normalizing the atomic percentages of the detected chemical states to the atomic percent of oxidized metal (Al^{+3}, Ti^{+4}, and Si^{+4}).

TABLE 2 Concentrations of Atomic Species Detected by XPS for Plasma-etched Aluminum and Titanium Substrates, 8.0 nm Plasma-polymerized a-SiO_2 Primer Films on Aluminum and Titanium Substrates, and Pure a-SiO_2

Sample	Atomic composition		
Plasma-etched aluminum	33.5±1.7% Al^{+3}	47.9±2.4% O^2	18.6±0.9% OH
Plasma-etched titanium	26.4±1.3% Ti^{+4}	62.5±3.1% O^{2-}	11.1±0.6% OH
8.0 nm a-SiO_2 deposition on aluminum	28.6±1.4% Si^{+4}	67.5±3.4% O^{2-}	3.9±0.2% OH
8.0 nm a-SiO_2 deposition on titanium	28.6±1.4% Si^{+4}	66.7±3.3% O^{2-}	4.7±0.2% OH
Pure a-SiO_2 (quartz)	31.7±1.6% Si^{+4}	68.3±3.4% O^{2-}	0.0±0.0% OH

The oxide surface of the plasma-etched aluminum substrate had an O/Al ratio of 1.43 and had a slight excess of aluminum (Al^{+3}) when compared with a perfect stoichiometry of 1.5 for Al_2O_3. This was likely due to oxygen vacancies and hydroxyl groups that were present in the oxide. The O/Ti ratio of the plasma-etched titanium oxide showed an excess of oxygen (O^{2-}) and was likely due to either oxygen interstitial species, ion-induced oxygen defects from plasma etching, or both [8]. The compositions of the plasma-polymerized a-SiO_2 films also had excess network (O^{2-}) oxygen when compared with the quartz sample. The excess network oxygen in the plasma-polymerized films may have been due to the incorporation of oxygen interstitials and defects, similar to the oxide of plasma-etched titanium.

The O/Si ratio can be used to indicate the structural morphology of silica-like materials [3]. Three-dimensional a-SiO_2 networks have an O/Si ratio of two, whereas sheets and rings have O/Si ratios of 2.5 and 3, respectively [15]. If either sheet or ring structures were incorporated in the plasma-polymerized films, the O/Si ratio would increase. Ring structures having three and four silica tetrahedral units have been shown to occur in typical a-SiO_2 networks [16].

TABLE 3 Compositional Formulae for Plasma-etched Aluminum and Titanium Substrates, 8.0 nm Plasma-polymerized a-SiO_2 Primer Films on Aluminum and Titanium Substrates, and Pure a-SiO_2

Sample	Compositional formula
Plasma-etched aluminum	$Al_{1.0\pm0.02}\ O_{1.43\pm0.03}\ OH_{0.55\pm0.02}$
Plasma-etched titanium	$Ti_{1.0\pm0.01}\ O_{2.37\pm0.04}\ OH_{0.42\pm0.01}$
8.0 nm a-SiO_2 deposition on aluminum	$Si_{1.0\pm0.02}\ O_{2.36\pm0.09}\ OH_{0.14\pm0.00}$
8.0 nm a-SiO_2 deposition on titanium	$Si_{1.0\pm0.02}\ O_{2.33\pm0.08}\ OH_{0.16\pm0.00}$
Pure a-SiO_2 (quartz)	$Si_{1.0\pm0.02}\ O_{2.15\pm0.08}\ OH_{0.0\pm0.00}$

A significant result shown in Table 3 is that the thick a-SiO_2 film deposited on the titanium substrate had a nearly identical composition in comparison with the thick a-SiO_2 film deposited on the aluminum substrate. In addition, the infrared results in Part I of this work supported this. This indicated that even though more suboxide was formed at the a-SiO_2/titanium-oxide interface when compared with the a-SiO_2/aluminum-oxide interface, it had no significant long-range effects on the bulk composition or structure of a thick a-SiO_2 film. Adhesive bonding to plasma-polymerized a-SiO_2 primer films should occur independently of the substrate, whether it is aluminum or titanium, as long as the primer films are thicker than the suboxide layer at the a-SiO_2/metal interface.

Tables 4 and 5 show the concentrations of the atomic species detected at a 75° take-off angle for the 0.8 nm depositions on aluminum and titanium substrates, respectively. In comparison with the 2.4-nm thick depositions, these depositions were thinner than the fully developed suboxide region at the a-SiO_2/metal-oxide interface. The composition of these films was assumed to be representative of the molecular structure of the interfacial region between the oxide surface

TABLE 4 Concentrations of Atomic Species Detected by XPS for 0.8 nm Plasma-polymerized a-SiO_2 Primer Films on Aluminum and Titanium Substrates

	0.8 nm deposition	
Atomic species	Aluminum substrate	Titanium substrate
Al^{+3}, Ti^{+4}	18.4±0.92	12.5±0.63
Si^{+4}	13.0±0.65	5.64±0.28
Si^{+3}	5.63±0.28	8.08±0.40
O^{2-} (Al, Ti)	20.9±1.04	28.3±1.42
O^{2-} (Si)	40.3±2.02	33.0±1.65
OH (Si)	1.86±0.09	1.64±0.08

TABLE 5 Compositional Formulae for 0.8 nm Plasma-Polymerized a-SiO_2 Primer Films on Aluminum and Titanium Substrates

Sample	Compositional formula
0.8 nm a-SiO_2 deposition on aluminum	$[Al_{1.00\pm0.01}\ O_{1.14\pm0.02}\ OH_{0.00}]$ $[Si_{1.00\pm0.01}\ O_{2.16\pm0.04}\ OH_{0.10\pm0.00}]$
0.8 nm a-SiO_2 deposition on titanium	$[Ti_{1.00\pm0.01}\ O_{2.26\pm0.03}\ OH_{0.86\pm0.01}]$ $[Si_{1.00+0.01}\ O_{2.40\pm0.03}\ OH_{0.12\pm0.00}]$

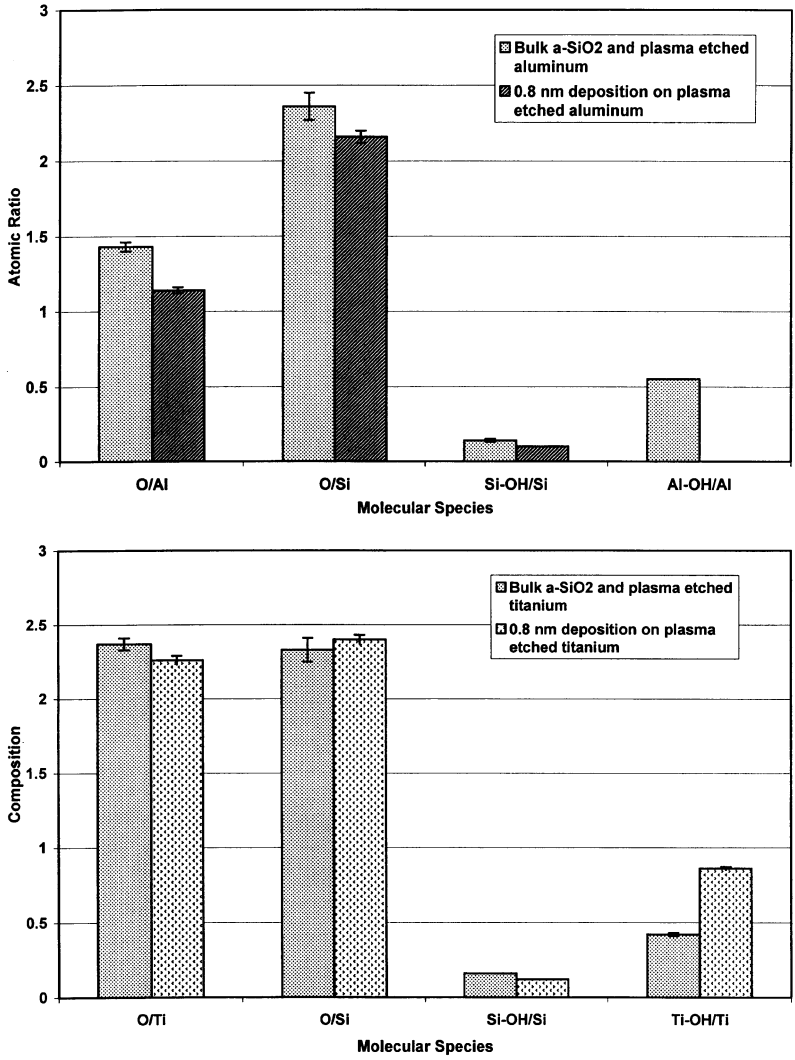

FIGURE 12 Atomic ratios of the 0.8 nm a-SiO_2 films on aluminum and titanium substrates compared with bulk a-SiO_2 and their corresponding plasma-etched substrates.

of the metal substrates and the first few molecular layers of the a-SiO_2 primer film.

Figure 12 shows a graphical summary of the atomic ratios for the 0.8 nm a-SiO_2 films along with their plasma-etched substrates that

were listed in Tables 2 and 3. Figure 12 shows that some structural changes occurred in the a-SiO_2 film and the plasma-etched substrate upon deposition. A small decrease in the oxygen/metal ratio was observed after depositing a-SiO_2 on aluminum and titanium substrates. In the case of the titanium substrate, the small decrease in the oxygen/metal ratio was consistent with the increase in titanium hydroxyl formation. The same effect was not observed for the aluminum substrate and, instead, no hydroxyls could be detected. This was due to the fact that the O^{2-}/OH peak separation for titanium was greater than that of aluminum, and the aluminum hydroxyl component in the O(1s) spectra for the 0.8 nm a-SiO_2 film deposited on aluminum could not be resolved. Based on the observed increase in titanium hydroxyl groups, it can be safely assumed that the same increase occurred for the case of aluminum.

The increase in metal hydroxyl formation at the a-SiO_2/metal-oxide interface was most likely due to the oxidation and then hydroxylation of the metal atoms drawn to the a-SiO_2/metal-oxide interface during deposition. Since silicon suboxide is formed by a thermodynamically favored oxidation of the metal atoms, it seems likely that some of the oxidized metal would form hydroxyl groups. The in situ infrared results showed that metal oxidation occurred to form Al-O and Ti-O bonds; however, since the Si-OH and metal hydroxyl groups had similar absorption frequencies, a small increase in metal hydroxyl at the a-SiO_2/metal-oxide interface could not be determined.

One explanation that accounts for the increase in hydroxyl groups at the a-SiO_2/metal interface is the formation of Ti-O-Si and Al-O-Si bonds. The O(1s) binding energies of the oxygen atoms for these bonds are between the O(1s) binding energies of the a-SiO_2 and the metal oxide [17]. This additional O(1s) peak component due to Al-O-Si or Ti-O-Si would be superimposed upon the Al-OH and Ti-OH peak, respectively. The additive effect would lead to an increase in the Ti-OH and Al-OH peak intensities and may be interpreted as an increase in hydroxyl concentration. The formation of Al-O-Si and Ti-O-Si bonds was consistent with the decrease in the O/Al and O/Ti ratios and the decrease in the O/Si ratio for the a-SiO_2/aluminum-oxide interface, but a significant change in the O/Si ratio at the a-SiO_2/titanium-oxide interface could not be determined within error.

The reduction of the O/Si ratio from 2.36 to 2.16 at the a-SiO_2/aluminum-oxide interface was also consistent with the inclusion of 30% suboxide. However, unlike the 0.8 nm deposition on aluminum, no change in the O/Si ratio of the a-SiO_2/titanium-oxide interface compared with the bulk a-SiO_2 film could be determined within error. Because of the higher amount of suboxide at the

a-SiO_2/titanium interface, a larger decrease in the O/Si ratio was expected. This inconsistency was likely due to the various types of nonbridging oxygen defects in a-SiO_2 that had a significant effect on the O(1s) peak component for the a-SiO_2 film. This was expected to be especially true of the 0.8 nm a-SiO_2 films on titanium because of their high concentration of Si^{+3} suboxide defects.

In order to interpret further the structure at the a-SiO_2/metal-oxide interface, the reaction mechanisms that govern the deposition of a-SiO_2 from organosiloxane monomers, such as HMDSO, must be considered. Several studies involving residual gas mass spectroscopy have been carried out in order to determine the molecular processes that drive plasma deposition of organosiloxane monomers such as HMDSO in oxygen [18–21]. These studies have shown that, when injected into the plasma, the monomer molecules become ionized due to scission of Si-C bonds according to the following reactions [18]:

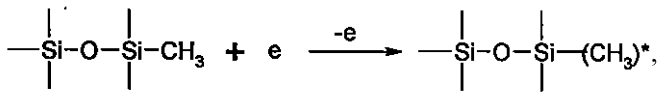

(3)

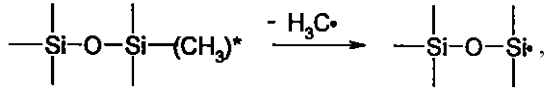

(4)

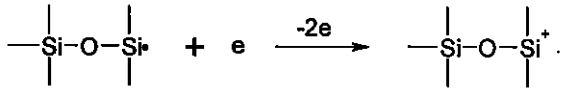

(5)

Collisions from energetic electrons in the plasma will cause homolytic scission of the Si-CH_3 bond. Further interaction with the electrons in the plasma results in the loss of an electron by the monomer radical. This forms a positively charged ionic species, which is energetically favored [18]. The monomer fragments shown above have also been shown to oligomerize by the following reaction [19]:

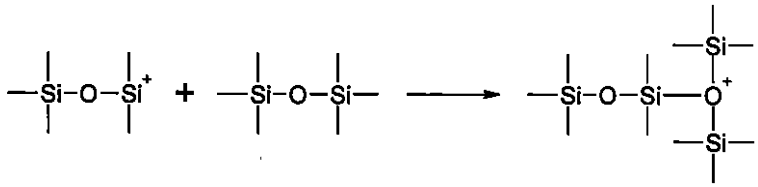

(6)

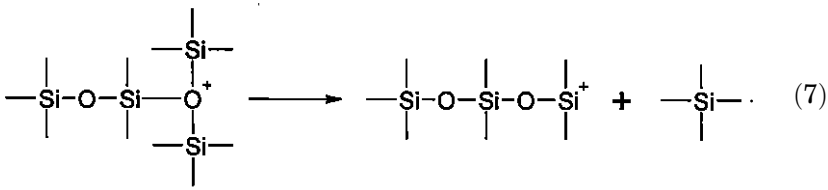

(7)

The positively charged oligomer and monomer molecules are attracted to and deposit on plasma-exposed surfaces, where they undergo polymerization and further ionization. When oxygen is present in the plasma, the organic components of the deposited species are oxidized into gaseous combustion-like products (H_2O, CO_2, and CO) and Si-O-Si network bonds are created [20].

If the ionic portion of the monomer molecule does not fully oxidize when the molecule becomes incorporated and buried in the growing a-SiO_2 network, then the Si^{+3} suboxide will be preserved. Concurrent oxidation of metal atoms at the a-SiO_2/metal interface during deposition would hinder or prevent oxidation of the adsorbed monomer molecules since the formation of the metal oxides are more thermodynamically favorable. As deposition proceeds, monomer molecules compete with metal atoms for atomic oxygen, and silicon atoms with a +3 oxidation state remain trapped at the a-SiO_2/metal oxide interface.

Figure 13 shows the possible reaction schemes (left and right side) for preferential metal oxidation in the presence of the ionized monomer and atomic hydrogen (top). These reactions reflect the results shown in Figure 12 and the discussions above. The reaction on the left produces a metal hydroxyl, the suboxide, and a hydrogen bond between the metal hydroxyl and a bridging oxygen atom of the monomer or a-SiO_2 network. The reaction path on the right side indicates primary bond formation between the metal oxide and the silicon atom. The metal hydroxyl group on the left can also react with the silicon ion to produce a primary bond, which is shown by the additional reaction path from the left to the right. Either reaction may have occurred during plasma deposition of a-SiO_2 on aluminum or titanium, but the overall results of this study, as well as thermodynamic considerations, supported the reaction on the right, which formed primary bonds. Additional support for the formation of primary bonds between the a-SiO_2 film and the metal substrate was due, in part, to the indeterminably high cohesive strengths and hydration resistance exhibited by the a-SiO_2/aluminum-oxide and a-SiO_2/titanium-oxide interfaces, which were determined in Part III of this work and in other studies [22, 23].

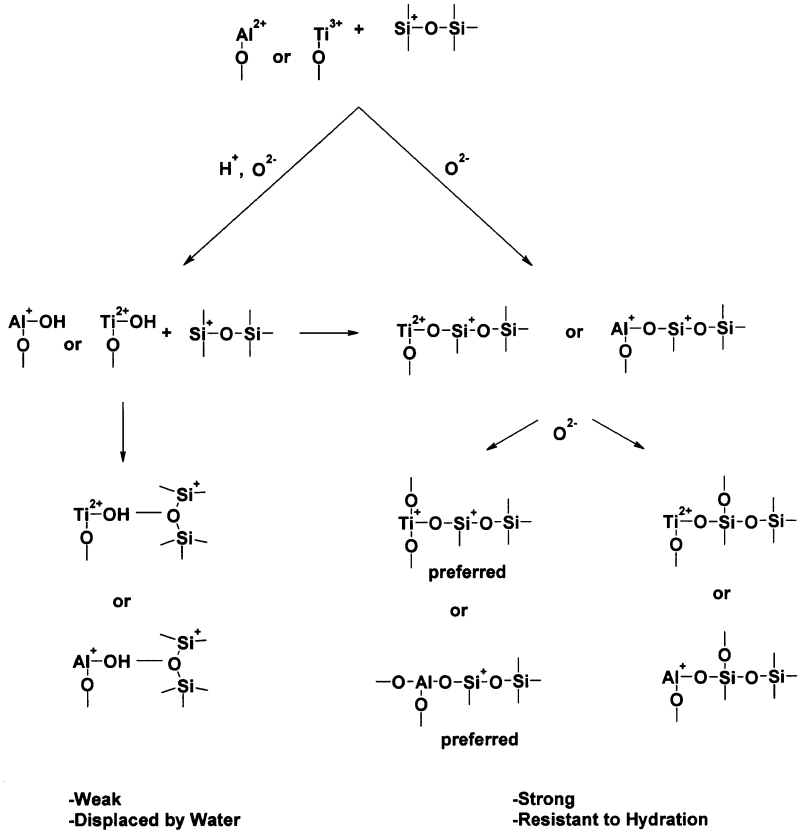

FIGURE 13 Reactions between plasma ionized HMDSO monomer molecule with titanium atoms that are not fully oxidized in the presence of atomic oxygen and hydrogen. The methyl groups on the monomer molecule have been omitted for clarity.

If the a-SiO_2/metal-oxide interface formed without Al-O-Si bonds or Ti-O-Si bonds, then the adhesion of the a-SiO_2 film to the metal-oxide would be due to dispersion forces and hydrogen bonding between the primer film and metal oxide (left side reactions in Figure 13). This hydrogen-bonded a-SiO_2 film would have a sheetlike structure similar to clay minerals such as kaolinite, which consist of layers of sheetlike silicates that are hydrogen bonded together [3]. The mechanical and durability strengths of the a-SiO_2/metal interface do not support a hydrogen-bonded sheetlike a-SiO_2 film, since the adhesion of a hydrogen-bonded oxide interface would be fairly weak and, like clay minerals, would not resist hydration.

Figure 13 also shows the effect of the valence difference between the aluminum and titanium atoms. Since aluminum has a smaller valence than titanium, one atom can have fewer interactions with the a-SiO_2 film to produce the suboxide species. This, in addition to the greater diffusion of the titanium atom to the a-SiO_2/metal-oxide interface, promoted the formation of more suboxide at the a-SiO_2/titanium-oxide interface.

The molecular structures of the 2.4-nm thick a-SiO_2 films that were deposited onto aluminum and titanium substrates were modeled and are shown in Figures 14 and 15. These two-dimensional models were constructed to be consistent with the primary bond reaction proposed in Figure 13, the depth results from modeling the XPS data, and the compositional formulae in Tables 3 and 4. Both models show intimate chemical bonding between the oxide of the metal substrate and the first deposited layer of a-SiO_2 film.

Because of its higher diffusivity and valence, titanium atoms produced more suboxide at the a-SiO_2/metal-oxide interface than aluminum. The a-SiO_2 film deposited onto the aluminum and titanium substrates had 1.0-nm and 1.6-nm thick suboxide regions, respectively, and were illustrated in Figures 14 and 15 to be 3 and 5 molecular layers thick, respectively, in agreement with the suboxide layer and thickness results. The amount of Si^{+3} in the suboxide layers for

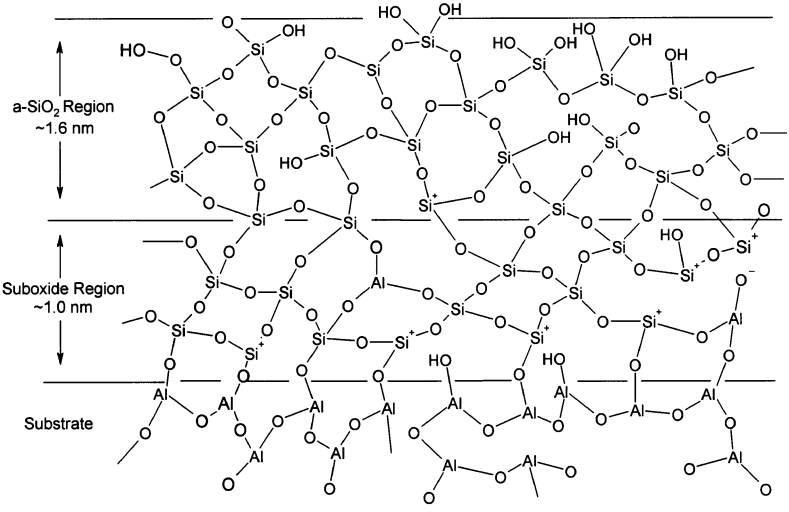

FIGURE 14 Model structure of a 2.4 nm a-SiO_2 film plasma polymerized onto an aluminum substrate.

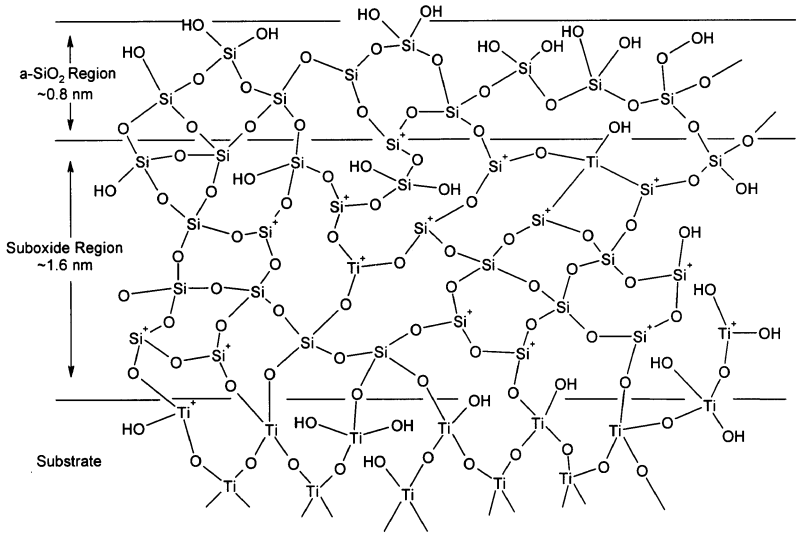

FIGURE 15 Model structure of a 2.4 nm a-SiO_2 film plasma polymerized onto a titanium substrate.

the 2.4 nm depositions on aluminum and titanium was 30 and 60%, respectively, which is in agreement with the atomic species concentrations shown in Table 4. These models represent the structure and composition of the a-SiO_2 primer films in terms of the spectroscopic results of this study.

In order to test the validity of the proposed interfacial models and the overall phenomena that leads to silicon suboxide formation, depositions were carried out on titanium substrates that had surfaces with various oxide thicknesses. Since titanium metal atoms were preferentially oxidized at the metal-oxide surface during plasma deposition and formed silicon suboxide, regulating the number of titanium atoms that migrate to the oxide surface will result in the formation of different amounts of silicon suboxide. This can be achieved by changing the thickness of the native oxide film. For example, depositing an a-SiO_2 film onto a titanium substrate with a thin oxide layer will produce more silicon suboxide due to a greater concentration of titanium atoms that migrate to the a-SiO_2/titanium-oxide interface. Similarly, a deposition on a very thick titanium oxide film should not produce suboxide, since little or no unoxidized titanium atoms can migrate to the oxide surface.

Very little difference in suboxide amounts were detected for a 2.4 nm deposition on a titanium substrate with a thin, 1.7 nm

titanium oxide layer, compared with a 2.4 nm deposition on a substrate that was argon/oxygen plasma etched for 10 min. However, depositions on the thicker titanium oxide layers that were formed by plasma etching with oxygen for 20 min and 60 min showed relatively less and no suboxide, respectively. The Si^{+4} and Si^{+3} peak area percentages of the curve-fitted Si(2p) spectra are plotted in Figure 16. This exercise showed that during deposition the silicon-suboxide formation on titanium depended on the oxide thickness of the titanium substrate. For an oxide thickness on a titanium substrate that is less than that obtained for the 10 min plasma etch, ca. 7 nm, the degree of suboxide formation was the same. This was due to the fact that the oxidation of the titanium substrate, for oxide thicknesses less than 7 nm, occurred much faster than the plasma deposition of a-SiO_2. For thicker oxide films on the titanium substrate, migration and oxidation of titanium atoms was much slower than the deposition rate of a-SiO_2, and less suboxide was formed. For the deposition on the very thick layer of titanium oxide, the migration and oxidation of titanium atoms was negligible, and no silicon suboxide was formed at the a-SiO_2/titanium-oxide interface.

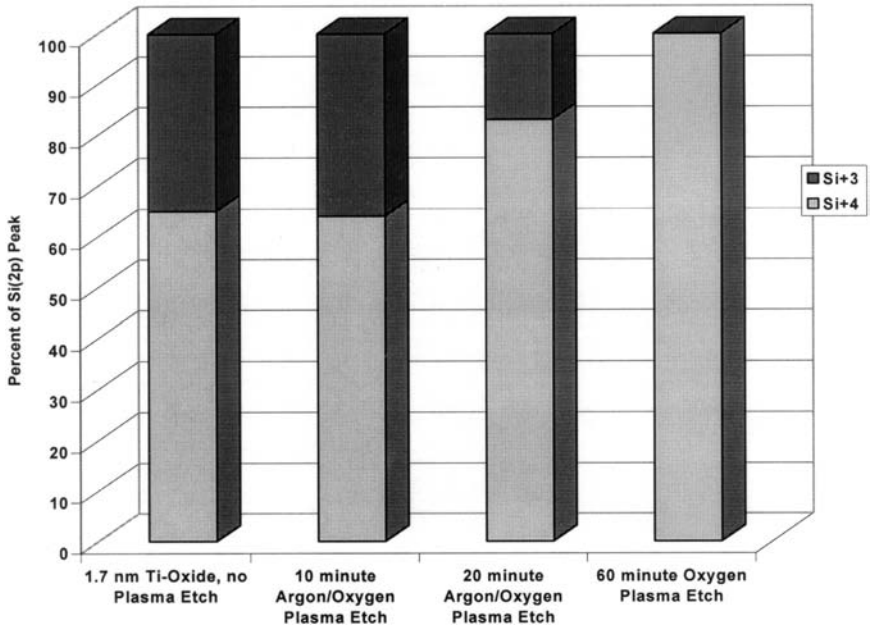

FIGURE 16 Plot of the Si^{+4} and Si^{+3} area contributions of 2.4 nm a-SiO_2 depositions on titanium substrates with various native oxide thicknesses.

CONCLUSIONS

A detailed analysis of the a-SiO_2 interface showed that intimate chemical reactions occurred at the a-SiO_2/metal-oxide interface for plasma-polymerized a-SiO_2 films on aluminum and titanium substrates. Metal atoms that diffused to the surface of the metal oxide film became oxidized and formed primary bonds with the monomer molecules at the a-SiO_2/metal-interface during plasma deposition. The oxidation/hydroxylation of metal atoms at the metal-oxide surface was thermodynamically preferred over the oxidation of depositing monomer molecules and, as a result, full oxidation of the depositing monomer species was not achieved. This resulted in a $+3$ oxidation state for some of the silicon atoms. As deposition continued, the transport of metal atoms decayed with increasing a-SiO_2 film thickness and left the under-oxidized silicon atoms buried beneath fully oxidized a-SiO_2.

The silicon suboxide species analyzed by in situ RAIR had a logarithmic growth rate similar to that for low-temperature oxidation of metals such as aluminum and titanium. This type of oxidation rate is known to be controlled by the diffusion of the atomic species in the oxide film and is driven by an electric field created across the oxide layer. When the diffusivities of aluminum and titanium were compared in Part I of this work, it was found that metal atoms diffuse more readily in titanium oxide than in aluminum oxide. This was consistent with thickness differences of the oxide layers on the as-polished and plasma-etched aluminum and titanium substrates.

Mathematical modeling of the XPS results gave depth information for atomic species and indicated that the regions containing the suboxide species were different in thickness depending on the substrate, aluminum or titanium. This was also consistent with the difference in atom diffusivities between aluminum and titanium in their respective oxides, since it was found that the suboxide layer for depositions on aluminum was approximately three atomic layers thick (ca. 1.0 nm), and for depositions on titanium the suboxide layer was five atomic layers thick (ca. 1.6 nm). The degree of Si^{+3} suboxide formation was also greater for depositions on titanium than for aluminum since the valence of titanium was higher than aluminum.

The formation of silicon suboxide species at the a-SiO_2/metal-oxide interface by oxidation of migrating metal atoms during initial stages of deposition was investigated by carrying out depositions on titanium substrates with various oxide thicknesses. By varying the substrate oxide thickness the migration of metal atoms was varied, and, for a thick oxide film it was prevented completely. Because of this, varying

the oxide thickness of the substrate essentially regulated the amount of suboxide that was formed at the a-SiO_2/metal-oxide interface. This result supported the proposed mechanisms for the formation of silicon suboxide at the a-SiO_2/metal-oxide interface.

The analysis of the compositions of 0.8 nm a-SiO_2 films indicated that Al-O-Si and Ti-O-Si bonds were formed at the a-SiO_2/metal-oxide interface. Due to the fact that the metal-hydroxyl peak and the Ti-O-Si peak overlap, this may alternately be interpreted as an increase in metal-hydroxyl groups at the a-SiO_2/metal-oxide interface. However, this alternate interpretation did not agree with the macroscopic properties of the a-SiO_2/metal-oxide interface and was rejected in favor of primary Al-O-Si and Ti-O-Si bond formation.

Models of the molecular structure at the a-SiO_2/metal-primer interface were constructed and were consistent with the in situ RAIR and in situ XPS analysis. These models showed that primary bonding occurred between the a-SiO_2 primer and the surface of the metal substrate. The model structure of the suboxide region was shown to be two molecular layers thicker for depositions on titanium substrates than on aluminum substrates.

REFERENCES

[1] Himpsel, F. J., McFeely, F. R., Taleb-Ibrahimi, A., Yarmoff, J. A., and Hollinger, G., *Phys. Rev. B* **38**, 6084–6096 (1988).
[2] Palik, E. D., Ed., *Handbook of Optical Constants of Solids* (Academic Press, Orlando, FL, 1988).
[3] Kingery, W. D., Bowen, H. K., and Uhlmann, D. R., *Introduction to Ceramics* (Wiley, New York, 1976), 2nd ed.
[4] Wagner, C. P., Riggs, W. M., Davis, L. E., Moulder, J. F., and Muilenberg, G. E., in *Handbook of X-ray Photoelectron Spectroscopy* (Perkin-Elmer, Eden Prairie, MN, 1979).
[5] Strohmeier, B. R., *Surf. Interface Anal.* **15**, 51–56 (1990).
[6] Carlson, T. A., *Surf. Interface Anal.* **4** 125–134 (1982).
[7] Seah, M. P. and Dench, W. A., *Surf. Interface Anal.* **1**, 2–10 (1979).
[8] McCafferty, E. and Wightman, J. P., *Surf. Interface Anal.* **26**, 549–564 (1998).
[9] Weast, R. C., Ed., *Handbook of Chemistry and Physics* (CRC Press, Boca Raton, FL, 1984), 65th ed., pp. B68–B69.
[10] Pasquarello, A., Hybertsen, M. S., and Car, R., *Phys. Rev. B* **53**, 10942–10950 (1996).
[11] Spruytte, S., Coldren, C., Harris, J., Pantelidis, D., Lee, H.-J., Bravman, J., and Kelly, M., *J. Vac. Sci. Technol. A* **19**, 603–608 (2001).
[12] Ro, C.-U., *Surf. Interface Anal.* **25**, 869–877 (1997).
[13] Williams, J. M. and Beebe, T. P., Jr., *J. Vac. Sci. Technol. A* **15**, 2122–2213 (1997).
[14] Powell, C. J. and Seah, M. P., *J. Vac. Sci. Technol. A* **8**, 735–763 (1990).
[15] Liebau, F., *Structural Chemistry of Silicates* (Springer-Verlag, New York, 1985), p. 96.
[16] Galeener, F. I., *Solid State Comm.* **44**, 1037–1040 (1982).

[17] Barr, T. L., *J. Vac. Sci. Technol. A* **9**, 1793–1805 (1991).
[18] Wrobel, M. and Wertheimer, M. R., in *Plasma Deposition, Treatment, and Etching of Polymers*, d'Agostino, R., Ed. (Academic Press, Boston, MA, 1990), Chap. 3.
[19] Alexander, M. R., Jones, F. R., and Short, R. D., *J. Phys. Chem. B* **101**, 3614–3619 (1997).
[20] Magni, D., Deschenaux, C., Hollenstein, C., Creatore, A., and Fayet, P. *J. Phys. D*, **34**, 87–94 (2001).
[21] Bourreau, C., Catherine, Y., and Garcia, P., *Mater. Sci. and Eng.* **A139**, 376–379 (1991).
[22] Turner, R. H., Segal, I., Boerio, F. J., and Davis, G. D., *J. Adhesion* **62**, 1–21 (1997).
[23] Taylor, C. E., Boerio, F. J., Ward, S. M., Ondrus, D. J., Dickie, R. A., and Brutto, M. M., *J. Adhesion* **69**, 237–261 (1999).